Advances in Applied Mathematics and Mechanics
Adv. Appl. Math. Mech., Vol. **5**, No. 3, pp. 321-336

DOI: 10.4208/aamm.12-m12116
June 2013

Natural Convection in a Concentric Annulus: A Lattice Boltzmann Method Study with Boundary Condition-Enforced Immersed Boundary Method

Yang Hu[1], Xiao-Dong Niu[1,2], Shi Shu[1,*], Haizhuan Yuan[1] and Mingjun Li[1]

[1] *School of Mathematics and Computational Science, Xiangtan University, Hunan, China*
[2] *Energy Conversion Research Center, Doshisha University, Kyoto, Japan*

Received 14 September 2012; Accepted (in revised version) 19 November 2012

Available online 30 April 2013

Abstract. In this paper, a boundary condition-enforced IBM is introduced into the LBM in order to satisfy the non-slip and temperature boundary conditions, and natural convections in a concentric isothermal annulus between a square outer cylinder and a circular inner cylinder are simulated. The obtained results show that the boundary condition-enforced method gives a better solution for the flow field and the complicated physics of the natural convections in the selected case is correctly captured. The calculated average Nusselt numbers agree well with the previous studies.

AMS subject classifications: 76R10

Key words: Lattice Boltzmann method, boundary condition-enforced immersed boundary method, natural convection.

1 Introduction

Natural convection is a flow process driven by temperature gradient on the gravity condition. Natural convection phenomena exist widely in engineering field, such as air refrigeration, solar energy storage, electronic component cooling and so on. Therefore it has attracted a large amount of attention about the characteristics of flow and heat transfer from researchers. Nowadays there are three basic methods that have been used to study this problem: theoretical analysis, experimental study and numerical simulation. Among them, numerical simulation is popular due to its low cost, efficiency and informativeness. Actually, there are many works to simulate natural convection problems

*Corresponding author.
Email: shushi@xtu.edu.cn (S. Shu)

using numerical method, especially the natural convection in enclosed spaces. As early as 1983, G Davis published a benchmark solution for natural convection in a square cavity [1]. Later many researchers have studied the natural convection problem in different cases by different methods [2–6].

Recently, a lattice Boltzmann method (LBM), as an alternative method of computational fluid dynamics, has been applied to many areas of fluid dynamics and heat transfer such as natural convection [7–13]. For example, Shu et al. applied LBM to simulate natural convection in a square cavity [7]. Dixit et al. computed the cases of high Rayleigh number natural convection [8]. Peng et al. developed a thermal LBM model to simulate 3D natural convection [10]. Nor Zwadi et al. proposed a Double-Population Thermal LBM to simulate natural convection [11]. Especially, some researchers have studied the natural convection in a concentric annulus using LBM. Peng et al used LBM to simulate natural convection in a concentric annulus between a square outer cylinder and a circular inner cylinder [12]. Shi et al. proposed a finite difference-based LBM to simulate natural convection heat transfer in a horizontal concentric annulus [13].

LBM is a particle-based numerical method at a mesoscopic level. The main advantage of LBM is its simplicity, and easily parallel computing and program coding, moreover setting the boundary condition is simple for LBM. After two decades' development, although the basic theory has been gradually improved, LBM encounters a challenge in simulating fluid problems with complex boundaries because it is based on Cartesian grid. In order to solve this problem, Feng and Michaelides [14] proposed a direct-forcing-boundary-LBM method by introducing Peskin's immersed Boundary method (IBM) [15] into LBM. IBM uses a fixed Eulerian grid in the flow field areas, and set up another set of Lagrangian points to represent objects immersed in the flow field. IBM can be naturally combined with LBM in deal with fluid flows with complex geometries due to both based on Cartesian grid. However, in the early IBM-LBM work [14], the interaction force between fluid and particles is computed by the penalty method which introduces a user-defined spring parameter. To overcome this drawback, Feng and Michaelides [16] later introduced a direct-forcing scheme and Niu et al. [17] proposed a momentum exchange-based IB-LBM for simulation of particles moving in incompressible flow.

Although the direct forcing and momentum-exchange ideas are simple and physically plausible, the non-slip boundary condition is often unable to be satisfied. The direct consequence of them is that streamlines penetrate the immersed boundary. So it is difficult to directly apply in thermal boundary. Recently, Shu et al. developed a boundary condition-enforced IBM to overcome the above drawbacks by solving the Navier-Stokes equations to study the natural convection problem [18]. This method has several advantages such as satisfying the non-slip condition, and introducing a little work to extend the method to thermal boundary including Dirichlet boundary and Neumann boundary. In the present study, the boundary condition-enforced IBM is further introduced to LBM, and the natural convections in a concentric isothermal annulus between a square outer cylinder and a circular inner cylinder are simulated. We use LBM as a fluid field solver and thermal field solver, and make use of the boundary condition-enforced IBM to deal

with the cylinder boundary. All results obtained are verified by comparing with those obtained by other researchers [18, 19].

2 Numerical methods

2.1 Governing equations

Under conditions of natural convection, buoyancy processing often uses the Boussinesq approximation. Therefore, macroscopic governing equations for this problem can be written as:

$$\nabla\cdot\mathbf{u}=0, \tag{2.1a}$$

$$\rho\Big(\frac{\partial\mathbf{u}}{\partial t}+\mathbf{u}\cdot\nabla\mathbf{u}\Big)=-\nabla p+\mu\nabla^2\mathbf{u}-\rho g(1-\beta(T-T_\infty))\mathbf{j}+\mathbf{f}, \tag{2.1b}$$

$$\rho c_p\Big(\frac{\partial T}{\partial t}+\mathbf{u}\cdot\nabla T\Big)=\kappa\nabla^2 T+q, \tag{2.1c}$$

with the boundary conditions on the boundary Γ:

$$\mathbf{u}_\Gamma=\mathbf{U}_{B\Gamma}, \tag{2.2a}$$

$$T_\Gamma=T_{B\Gamma}, \tag{2.2b}$$

where ρ, $\mathbf{u}$, p, T represent density, velocity, pressure and temperature, $\mathbf{u}_B$, T_B are velocity and temperature on the solid boundary; physical parameter μ, c_p, κ are dynamics viscosity, specific heat capacity at constant pressure and thermal conductivity, respectively; T_∞ is the reference temperature and β is the thermal expansion coefficient at the reference temperature; g is the gravitational acceleration directed downward, $\mathbf{j}$ is the unit positive-direction vector directed upward and $\mathbf{f}$ and q denote the external force and heat source terms.

2.2 Lattice Boltzmann method for flow and temperature fields

LBM governing equation with extern forcing term can be written as:

$$f_\alpha(\mathbf{x}+\mathbf{e}_\alpha\delta t,t+\delta t)-f_\alpha(\mathbf{x},t)=-\frac{1}{\tau_f}(f_\alpha(\mathbf{x},t)-f_\alpha^{eq}(\mathbf{x},t))+F_\alpha\delta t, \tag{2.3a}$$

$$g_\alpha(\mathbf{x}+\mathbf{e}_\alpha\delta t,t+\delta t)-g_\alpha(\mathbf{x},t)=-\frac{1}{\tau_g}(g_\alpha(\mathbf{x},t)-g_\alpha^{eq}(\mathbf{x},t))+Q_\alpha\delta t, \tag{2.3b}$$

where $\mathbf{x}$ and t are the coordinate of Eulerian node and time, and $f_\alpha(\mathbf{x},t)$ and $g_\alpha(\mathbf{x},t)$ denote density distribution function and thermal distribution function for the discrete velocity $\mathbf{e}_\alpha$, respectively; δt is time step, τ_f and τ_g are dimensionless relaxation times of

flow and temperature fields, respectively. $f_\alpha^{eq}(\mathbf{x},t)$ and $g_\alpha^{eq}(\mathbf{x},t)$ are the respective local equilibrium density and thermal distributions, and they can be expressed as

$$f_\alpha^{eq}(\mathbf{x},t)=\omega_\alpha\rho\Big(1+\frac{\mathbf{e}_\alpha\cdot\mathbf{u}}{c_s^2}+\frac{(\mathbf{e}_\alpha\cdot\mathbf{u})^2}{2c_s^4}-\frac{\mathbf{u}^2}{2c_s^2}\Big), \tag{2.4a}$$

$$g_\alpha^{eq}(\mathbf{x},t)=\omega_\alpha T\Big(1+\frac{\mathbf{e}_\alpha\cdot\mathbf{u}}{c_s^2}+\frac{(\mathbf{e}_\alpha\cdot\mathbf{u})^2}{2c_s^4}-\frac{\mathbf{u}^2}{2c_s^2}\Big), \tag{2.4b}$$

where c_s is the lattice sound speed and ω_α is the weight coefficients which depend on lattice velocity model.

In our study, D2Q9 a model has been used, the velocity set is defined as:

$$\mathbf{e}_\alpha=\begin{cases}0, & \alpha=0,\\ \Big(\cos\Big[(\alpha-1)\dfrac{\pi}{2}\Big],\sin\Big[(\alpha-1)\dfrac{\pi}{2}\Big]\Big)c, & \alpha=1,2,3,4,\\ \sqrt{2}\Big(\cos\Big[(2\alpha-1)\dfrac{\pi}{4}\Big],\sin\Big[(2\alpha-1)\dfrac{\pi}{4}\Big]\Big)c, & \alpha=5,6,7,8,\end{cases} \tag{2.5}$$

where $c=\delta x/\delta t$, δx is the lattice spacing. Further, $c=\sqrt{3}c_s$. In the case of $\delta x=\delta t$, c is taken as 1. The corresponding weight coefficients are given as:

$$c=\begin{cases}\dfrac{4}{9}, & \alpha=0,\\ \dfrac{1}{9}, & \alpha=1,2,3,4,\\ \dfrac{1}{36}, & \alpha=5,6,7,8.\end{cases} \tag{2.6}$$

The discrete force term $\mathbf{F}_\alpha$ in Eq. (2.4a) is defined as:

$$\mathbf{F}_\alpha=\Big(1-\frac{1}{2\tau}\Big)w_\alpha\Big(3\frac{\mathbf{e}_\alpha-\mathbf{u}}{c^2}+9\frac{\mathbf{e}_\alpha\cdot\mathbf{u}}{c^2}\Big)\cdot\mathbf{F}, \tag{2.7}$$

where $\mathbf{F}$ is a total external force which contains the forces come from immersed boundary and buoyancy. In our study, it is

$$\mathbf{F}=-\rho g\beta(T-T_\infty)\mathbf{j}+\mathbf{f}. \tag{2.8}$$

The heat source term Q_α in Eq. (2.3b) is determined by:

$$Q_\alpha=\omega_\alpha q. \tag{2.9}$$

The macro density, velocity and temperature in the LBM can be calculated by:

$$\rho=\sum_\alpha f_\alpha, \tag{2.10a}$$

$$\mathbf{u}=\Big(\sum_\alpha\mathbf{e}_\alpha f_\alpha+\frac{1}{2}\mathbf{F}\delta t\Big)\Big/\rho, \tag{2.10b}$$

$$T=\sum_\alpha g_\alpha+\frac{1}{2}q\delta t. \tag{2.10c}$$

Using the Chapman-Enskog multi-scale analysis, we can deduced that the lattice Boltzmann equations (2.3a) and (2.3b) are consistent with the incompressible Navier-Stokes equations (2.1a)-(2.1c) to the second order of small Knudsen number with the relaxation times of τ_f and τ_g defined as:

$$\tau_f = 3\mu/(\rho c^2 \delta t) + 0.5, \tag{2.11a}$$

$$\tau_g = 3\kappa/(\rho c^2 \delta t) + 0.5. \tag{2.11b}$$

2.3 Velocity and temperature correction procedure

As previously mentioned, the boundary condition-enforced method [18] can satisfy non-slip condition and temperature condition, and this method has used for N-S solver [18]. In our study, this method will be extended to LBM solver. The boundary condition-enforced idea for the non-slip condition can be implemented as follows:

1. Velocity correction

Defining the intermediate velocity $\mathbf{u}^*$ as:

$$\mathbf{u}^* = \left(\sum_\alpha \mathbf{e}_\alpha f_\alpha - \rho g \beta (T - T_\infty)\mathbf{j}\right) \Big/ \rho, \tag{2.12}$$

and the velocity correction is calculated by

$$\delta\mathbf{u} = \frac{1}{2}\mathbf{f}\delta t/\rho. \tag{2.13}$$

Then the macro velocity can be written as:

$$\mathbf{u} = \mathbf{u}^* + \delta\mathbf{u}. \tag{2.14}$$

2. Calculating interaction force by the non-slip boundary condition

In the IBM [15], the interaction force f of the solid-fluid can be given by

$$\mathbf{f}(\mathbf{x},t) = \int_\Gamma \mathbf{F}(\mathbf{X}(s,t))\delta(\mathbf{x} - \mathbf{X}(s,t))ds, \tag{2.15}$$

where $\mathbf{X}$ is the coordinate of Lagrangian node on the immersed boundary, $\mathbf{F}(\mathbf{X}(s,t))$ is the force density at immersed boundary, and $\delta(\mathbf{x} - \mathbf{X}(s,t))$ denotes the Dirac delta function. The above equation can be further discretized by

$$\mathbf{f}(\mathbf{x}_i) = \sum_l \mathbf{F}(\mathbf{X}_B^l) D(\mathbf{x}_i - \mathbf{X}_B^l)\Delta s_l, \tag{2.16}$$

where Δs_l is the arc length of the boundary element, $\mathbf{X}_B^l$ $(l = 1,2,\cdots,M)$ are the discrete Lagrangian points on the immersed boundary, $\mathbf{x}_i$ $(i = 1,2,\cdots,N)$ are the uniform Cartesian

mesh points with mesh spacing $\delta x=\delta y=h$. $D(x_i-\mathbf{X}_B^l)$ is smoothly approximated of Dirac function, which is proposed by Peskin [15]:

$$\delta(r)=\begin{cases}\frac{1}{4}\big(1+\cos(\pi|r|/2)\big), & |r|\leq 2,\\ 0, & |r|>2,\end{cases} \tag{2.17a}$$

$$D_{il}=D(x_i-\mathbf{X}_B^l)=\delta(x_i-\mathbf{X}_B^l)\delta(y_i-\mathbf{Y}_B^l). \tag{2.17b}$$

From Eq. (2.16), one can see that the force term $\mathbf{f}(\mathbf{x}_i)$ at the Eulerian point is distributed from the boundary point. Eq. (2.16) can be further written in a matrix form as:

$$\mathbf{f}_E=A_{L\to E}\mathbf{F}_L, \tag{2.18}$$

with $A_{L\to E}$ be the matrix form of linear interpolation operator from Lagrangian points to Eulerian points:

$$A_{L\to E}=\begin{bmatrix} D_{11}\Delta s_1 & D_{12}\Delta s_1 & \cdots & D_{1N}\Delta s_1\\ D_{21}\Delta s_2 & D_{21}\Delta s_2 & \cdots & D_{21}\Delta s_2\\ \vdots & \vdots & \ddots & \vdots\\ D_{M1}\Delta s_M & D_{M2}\Delta s_M & \cdots & D_{MN}\Delta s_M\end{bmatrix}. \tag{2.19}$$

As at the Eulerian points, Eq. (2.13) gives

$$\mathbf{f}_E=2\rho\delta\mathbf{u}_E/\delta t. \tag{2.20}$$

Substituting Eq. (2.20) into Eq. (2.18), we can have

$$\delta\mathbf{u}_E=\frac{2\delta t}{\rho}A_{L\to E}\mathbf{F}_L. \tag{2.21}$$

According to the non-slip condition, the velocity at the boundary point is equal to the interpolated value from Eulerian points, that is

$$\mathbf{U}_L=h^2B_{E\to L}\mathbf{u}_E, \tag{2.22}$$

where

$$B_{E\to L}=\begin{bmatrix} D_{11} & D_{12} & \cdots & D_{1M}\\ D_{21} & D_{21} & \cdots & D_{21}\\ \vdots & \vdots & \ddots & \vdots\\ D_{N1} & D_{N2} & \cdots & D_{NM}\end{bmatrix}. \tag{2.23}$$

Substituting Eqs. (2.14) and (2.22) into Eq. (2.23), we can get the following algebraic equation system

$$\mathbf{U}_L=h^2B_{E\to L}\Big(\mathbf{u}_E^*+\frac{2\delta t}{\rho}A_{L\to E}\mathbf{F}_L\Big). \tag{2.24}$$

Algebraic equation (2.24) can be further written in the following form:

$$\frac{2\delta t h^2}{\rho} A_{L\to E} B_{E\to L} \mathbf{F}_L = \mathbf{U}_L - h^2 B_{E\to L} \mathbf{u}_E^*. \tag{2.25}$$

The boundary-enforced idea for temperature condition can be implemented as similarly as the velocity correction procedure.

1. Temperature correction

We define the intermediate temperature as:

$$T^* = \sum_\alpha g_\alpha, \tag{2.26}$$

and the temperature correction is calculated by

$$\delta T = \frac{1}{2} q \delta t. \tag{2.27}$$

On the basis of Eq. (2.14), the macro temperature on the immersed boundary can be expressed as:

$$T = T^* + \delta T. \tag{2.28}$$

2. Heat source calculation

The heat source term at the Eulerian point can interpolated from the heat flux of boundary point through the Dirac function, and can be written as:

$$q(\mathbf{x},t) = \int_\Gamma \delta Q(\mathbf{X}(s,t)) \delta(\mathbf{x} - \mathbf{X}(s,t)) ds, \tag{2.29}$$

with $\delta Q(\mathbf{X}(s,t))$ be the heat flux density on the immersed boundary. The matrix form of Eq. (2.29) is

$$q_E = A_{L\to E} \delta Q_L. \tag{2.30}$$

On the Eulerian points, similar to the velocity treatment, we can get the following equation:

$$q_E = 2\rho c_p / \delta t \delta T_E. \tag{2.31}$$

Substituting Eq. (2.31) into Eq. (2.30), we can get

$$\delta T_E = \frac{2\delta t}{\rho c_p} A_{L\to E} \delta Q_L. \tag{2.32}$$

To satisfy the temperature boundary condition, we should have

$$T_L = h^2 B_{E\to L} T_E. \tag{2.33}$$

Substituting Eqs. (2.29) and (2.32) into Eq. (2.33), we can obtain the following algebraic equation system:

$$T_L = h^2 B_{E\to L}\Big(T_E^* + \frac{2\delta t}{\rho c_p} A_{L\to E}\delta Q_L\Big). \tag{2.34}$$

Algebraic equation (2.34) can also be written in the following form:

$$\frac{2\delta t h^2}{\rho c_p} B_{E\to L} A_{L\to E}\delta Q_L = T_L - h^2 B_{E\to L} T_E^*. \tag{2.35}$$

By solving the algebraic equation systems (2.24) and (2.34), one can achieve the accurate velocity and temperature corrections. It is not difficult to find the elements of the coefficient matrix $A_{L\to E}$, $B_{E\to L}$, because the elements in $A_{L\to E}$, $B_{E\to L}$ are only depend on the coordinate information of immersed boundary and the adjacent points. So it increases a little workload to solve the fixed boundary problem.

3 Numerical examples

In this section, several different natural convection problems in a concentric annulus will be simulated by the proposed boundary condition-enforced LBM. In the study of natural convection problem, Rayleigh number and Prandtl number are very important parameters, and they are defined as:

$$\mathrm{Pr} = \frac{\mu c_p}{\kappa}, \qquad Ra = \frac{\rho^2 c_p \beta g L^3 (T_w - T_\infty)}{\kappa\mu}. \tag{3.1}$$

Here, T_w is the temperature on the inner cylinder surface. In order to compare with the former results, we selected the most representative Rayleigh number and Prandtl number of $Pr = 0.71$, $Ra = 10^4, 10^5, 10^6$.

In the present method, the relaxation times can not be expressed by Rayleigh number and Prandtl number directly. For easily calculation, we further introduce a characteristic velocity, $\mathbf{u}_{ref} = \sqrt{g\beta L(T_w - T_\infty)}$ and the Mach number, $Ma = \mathbf{u}_{ref}/c_s$, in the natural convection problems and the relaxation times of flow and temperature fields can be alternatively given as:

$$\tau_f = \sqrt{3\frac{\mathrm{Pr}}{Ra}}\frac{MaL}{\delta_t} + \frac{1}{2}, \tag{3.2a}$$

$$\tau_g = \sqrt{\frac{3}{Ra\mathrm{Pr}}}\frac{MaL}{\delta_t} + \frac{1}{2}. \tag{3.2b}$$

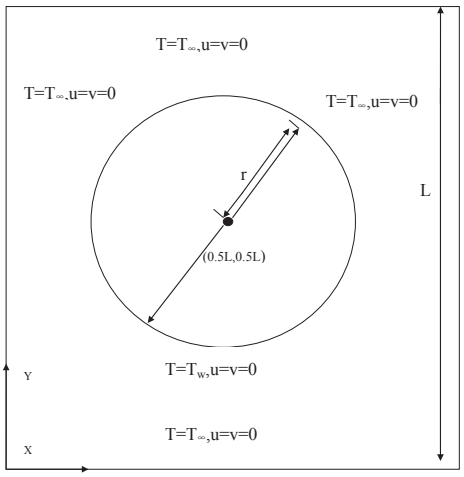

Figure 1: Configuration of natural convection in a concentric annulus between a square outer cylinder and a circular inner cylinder.

In our simulation, a two-dimensional incompressible natural convection flow is studied and problem is schematically described by Fig. 1. As shown in Fig. 1, the computational domain Ω contains a closed immersed boundary Γ, which divides the flow domain into internal and external areas. The initial conditions are set to zero for $\mathbf{u}$ and T_∞ for T in the entire domain, and the reference velocity $\mathbf{u}_{ref}$ is taken as 0.25 for all numerical cases. The numerical examples use the dimensionless form to compute, the side length of the outer cavity is taken as the reference length, and the temperature is normalized by

$$T^* = \frac{T - T_\infty}{T_w - T_\infty}. \tag{3.3}$$

For the purpose of the understanding the natural convection in a concentric annulus, the numerical cases of different aspect ratios $Ar = L/2r$ will be considered. In our study, the numerical cases of different Rayleigh numbers will be calculated with three aspect ratios of 5, 2.5 and 1.67. The heat transfer behaviors of the natural convection can be evaluated by Nusselt numbers. The local Nusselt number Nu is defined as:

$$Nu(\mathbf{X},t) = \frac{h(\mathbf{X},t)L}{\kappa}, \tag{3.4}$$

where $h(\mathbf{X},t)$ is heat convection coefficient, L is reference length. Based on the Newtons cooling law and Fouriers law, the average Nusselt number can be calculated by the following formula simply [18],

$$\overline{Nu} = \frac{1}{L}\int_\Gamma \frac{L_c}{\kappa(T_w - T_\infty)} Q(\mathbf{X}(s,t))ds. \tag{3.5}$$

In our study, L_c is taken as half of the circumferential length of the inner cylinder surface. So the discrete form of Eq. (3.5) can be written as:

$$\overline{Nu}=\frac{\sum_i Q_B^i \Delta s_i}{2\kappa(T_w-T_\infty)}. \tag{3.6}$$

In order to test the efficiency of the present method, the solution must be grid-independence. For the case of $Ra=10^5$, $Ar=2.5$, we use three different grids of 201×201, 251×251, 301×301. The results are listed in Table 1. As is shown in Table 1, the average Nusselt number has little change with the mesh refinement, so for the grid of 251×251, the solution is accurate enough. In our study, all the results are based on the grid of 251×251.

Table 1: The average Nusselt number computed by different grids for $Ra=10^5$, $Ar=2.5$.

Grid	201×201	251×251	301×301
$\overline{Nu}$	4.926	4.917	4.914

Figs. 2-4 show the numerical results visualized as the streamlines and isotherms. These figures can help us to effectively analyze the characteristics of flow, heat conduction and heat convection. Because the symmetry of physical conditions and geometry conditions, streamlines and isotherms are symmetrical about the central axis as shown in Figs. 2-4 clearly. As is shown in Fig. 2, it is the case of $Ra=10^4$, the isotherms are quasi-circular, implying that the heat flow in the cavity is dominated by diffusion, and the thermal convection is very weak. So it is not obvious that the velocity field affects the thermal field. With the change of the aspect ratio, Ar, the thermal boundary layer and the eddy will change obviously. The dynamic processes of natural convection shown in Fig. 2 are that two eddies are firstly originated in the cavity; when $Ar=5$, the eddy will move up, so the center of eddy moves above the horizontal axis; as Ar decreases from 5 to 2.5 and 1.67, each original eddy will split to two small eddies. Because of the buoyancy effect and the thermal boundary layer on the bottom surface of the cylinder thinner than that on its top surface.

With the Rayleigh number increases from 10^4 to 10^5, as shown in Fig. 3, the effect of convection are strengthen, so the closed isotherm and the center of eddy would move toward the y-axis positive direction. For the case of $Ar=2.5$, by the effect of buoyancy, the two small eddies under the horizontal disappear. When $Ar=1.67$, due to the space constraint, the flow field becomes more complicated with four large eddies and the central position of the top boundary appearing two small eddies.

As Rayleigh number increases further up to $Ra=10^6$ in Fig. 4, the isotherms strongly distorted and disordered, so the effect of convection increases stronglyit denote that the heat flow in annulus is mainly dominated by convection. The evolution of the flow field becomes more complex for the case of $Ar=5$ due to the vertical convection, strengthening near the cylindrical wall. The bottom of wall generates two secondary eddies. As aspect

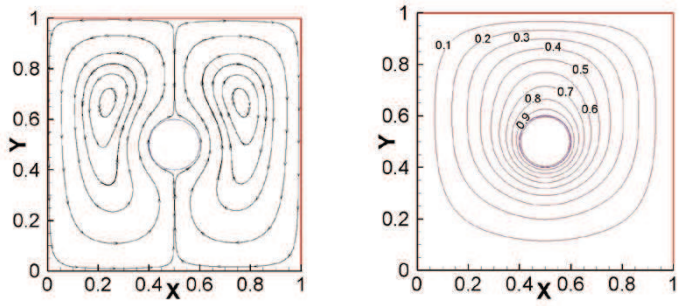

(a) $Ar = 5$

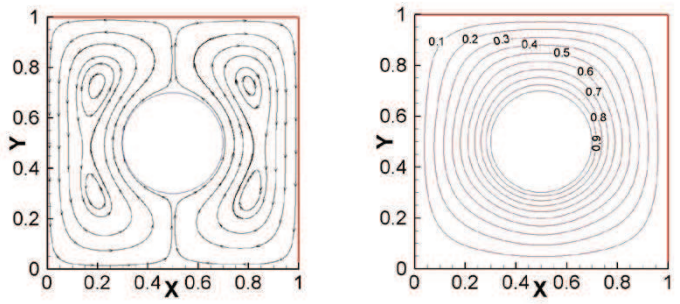

(b) $Ar = 2.5$

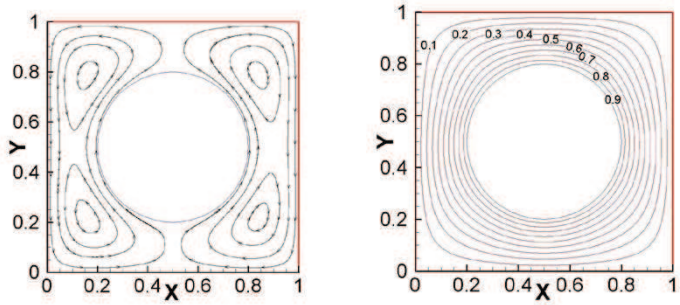

(c) $Ar = 1.67$

Figure 2: Streamlines (left) and isotherms (right) for $Ra = 10^4$.

ratio further decreases to 1.67, there exist six eddies. When compared with the case of $Ra = 10^5$, Fig. 4(c) shows that two eddies locate in the top of wall while the other four eddied on the left and right become more narrow and long. So in our study, due to the temperature and pressure differences and space constraints, natural convection in a concentric annulus produces different morphologies. With Rayleigh number increasing, the flow field and temperature field change from simple and laminar state to chaos.

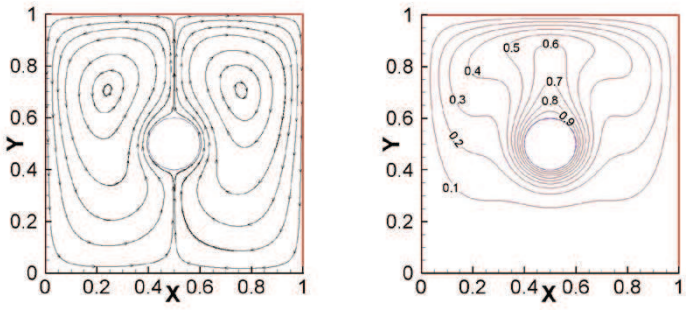

(a) $Ar = 5$

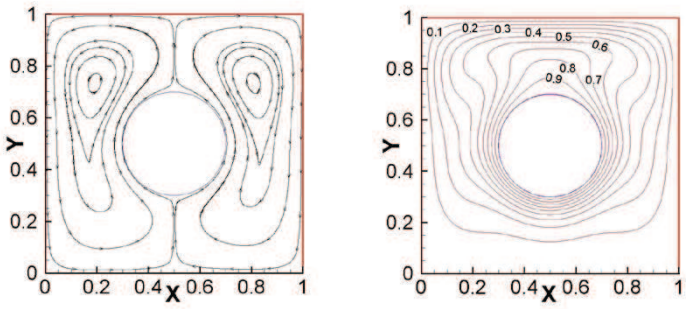

(b) $Ar = 2.5$

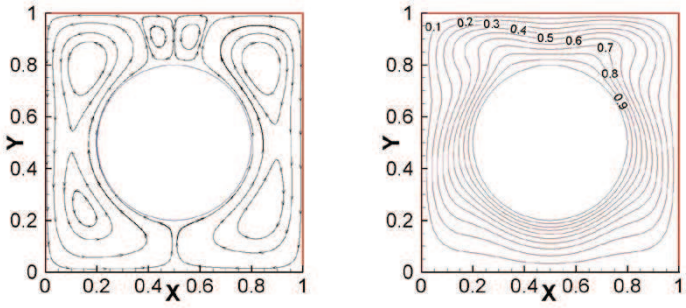

(c) $Ar = 1.67$

Figure 3: Streamlines (left) and isotherms (right) for $Ra = 10^5$.

In order to understand the details of flow, the forces density acting on the inner cylinder surface are shown in Figs. 5-8 with the angle starting from the top point of the inner cylinder and varying from 0° to 180° on the right half of the inner cylinder because of a two-fold symmetry about the vertical center line at $x = 0.5$. Figs. 5 and 6 show the force distributions on the inner cylinder in the respective x and y directions for the case of $Ar = 2.5$ at different Rayleigh numbers. As shown in Fig. 5, it is obvious that the distribu-

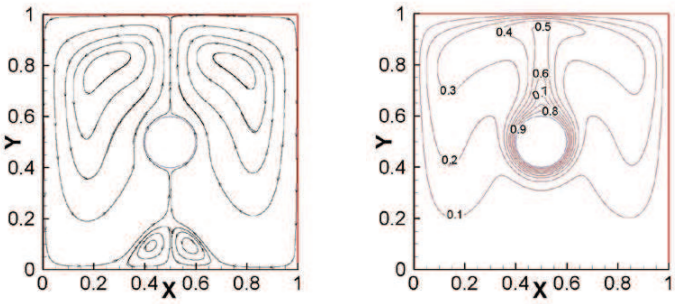

(a) $Ar = 5$

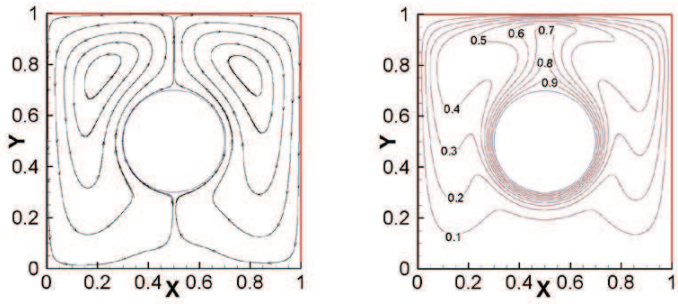

(b) $Ar = 2.5$

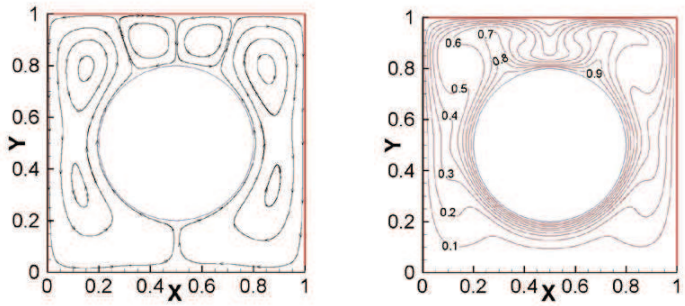

(c) $Ar = 1.67$

Figure 4: Streamlines (left) and isotherms (right) for $Ra = 10^6$.

tion of the forces on the inner cylinder in the x-direction is behaved like a Sine function. The amplitude of the force is larger around 50° and 140° than at other angles and also increases with increasing Rayleigh number from 10^4 to 10^6. In the y-direction as shown in Fig. 6, the distribution of forces is displayed like a Cosine function with a relative large value on the bottom point of the inner cylinder. It is clearly observed that there exists an up force due to the force difference between the lower and upper surfaces of the inner

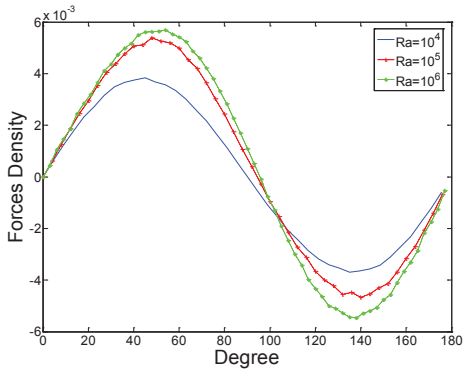

Figure 5: The force distributions acting on the inner cylinder in the x-direction at different Rayleigh number for $Ar=2.5$.

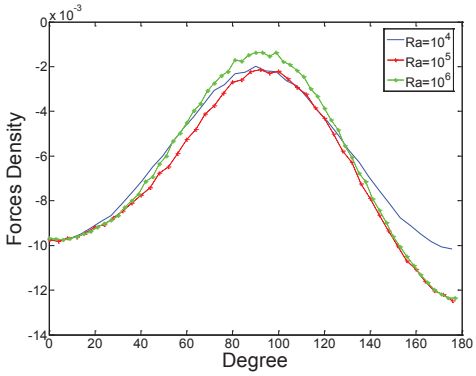

Figure 6: The force distributions acting on the inner cylinder in the y-direction at different Rayleigh number for $Ar=2.5$.

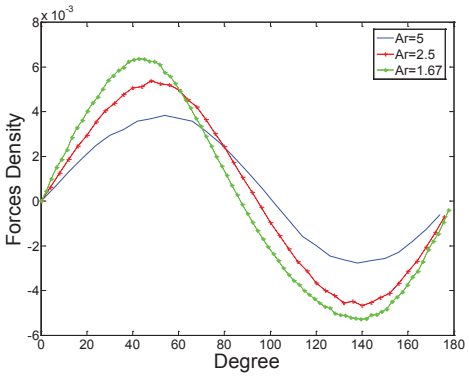

Figure 7: The force distributions acting on the inner cylinder in the x-direction at different aspect ratio for $Ra=10^5$.

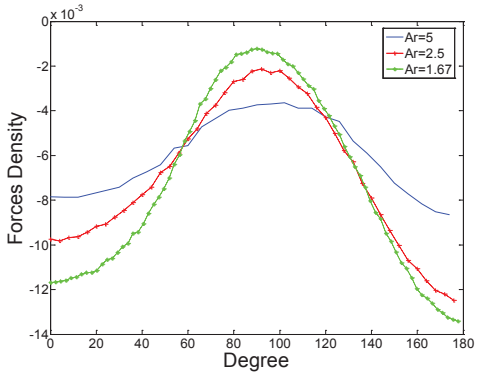

Figure 8: The force distributions acting on the inner cylinder in the y-direction at different aspect ratio for $Ra=10^5$.

cylinder. The values of the buoyance force acting on the inner cylinder in our simulation are 7.932×10^{-3}, 8.799×10^{-3}, 8.142×10^{-3} for $Ra=10^4$, 10^5, 10^6, respectively. These buoyance forces can be attributed to the contribution of the heat convection-induced the flow in the cavity. Figs. 7 and 8 show the force distributions on the inner cylinder in the respective x and y directions for the case of $Ra=10^5$ at different aspect ratios. As shown in Figs. 7 and 8, the amplitude of the force increases with aspect ratio increasing from 1.67 to 5. This is mainly due to the strong convection flow in the cavity with increasing Rayleigh number.

To verify the capacity of the current methods, we calculate the average Nusselt numbers and compare them with those given in [18,19]. The comparisons are listed in the Table 2. As is shown in the Table 2, decreasing the aspect ratio and increasing the Rayleigh number, the average Nusselt number increases, implying the heat transfer in the cavity is enhanced. The consistency of the present results to [18, 19] demonstrates that the

Table 2: Comparison of Computed average Nusselt numbers.

Cases		References		
Ra	*Ar*	Present	Ref. [18]	Ref. [19]
10^4	5	2.038	2.051	2.071
	2.5	3.184	3.161	3.331
	1.67	5.294	5.303	5.826
10^5	5	3.778	3.704	3.825
	2.5	4.917	4.836	5.080
	1.67	6.247	6.171	6.212
10^6	5	6.095	5.944	6.107
	2.5	8.934	8.546	9.374
	1.67	11.995	11.857	11.620

present boundary condition-enforced LBM is an efficient numerical tool in handling the numerical simulation of natural convection problems with complex geometries.

4 Conclusions

In this paper, a boundary condition-enforced IBM is introduced into the LBM and the solver is used to simulate the problem of natural convection in a concentric annulus. We use LBM as a fluid field solver and thermal field solver, and make use of the boundary condition-enforced IBM to deal with the cylinder boundary. The present method correctly captures the complicated physics of the natural convections in a concentric isothermal annulus between a square outer cylinder and a circular inner cylinder and all results obtained agree well with the previous studies.

Acknowledgments

This work was partially supported by the Key Project of Scientific Research Fund of Hunan Provincial Science and Technology Department (No. 2011FJ2011) in China, the Program for Changjiang Scholars and Innovative Research Team in University of China (No. IRT1179), the Scientific Research Fund of Hunan Provincial Education Department (No. 12A138) , the National Natural Science Fund of China (No. 11171281), the Hunan Provincial Innovation For PostGraduate (No. CX2012B264, No. CX2012B239), the One Hundred Person Project of Hunan Province of China under Xiangtan University, and the Academic Frontier Research Project on Next Generation Zero-emission Energy Conversion System of Ministry of Education, Culture,Sports, Science and Technology of Japan.

References

[1] G. D. V. DAVIS, *Natural convection of air in square cavity: a bench mark numerical solution*, Int. J. Numer. Methods Fluid, 3 (1983), pp. 249–264.

[2] J. C. PATTERSON AND S. W. ARMFIELD, *Transient features of natural convection in a cavity*, J. Fluid Mech., 219 (1990), pp. 469–497.
[3] M. HORTMANN, M. PERIC AND G. SCHEUERER, *Finite Volume multigrid prediction of laminar natural convection: Bench-Mark solutions*, Int. J. Numer. Methods Fluids, 11(2) (1990), pp. 189–207.
[4] B. V. K. S. SAI, K. N. SEETHARAMU AND P. A. A. NARAYANA, *Solution of transient laminar natural convection in a square cavity by an explicit finite element scheme*, Numer. Heat Trans., Part A Applications An Int. J. Comput. Methodology, 36(5) (1999), pp. 593–609.
[5] J. R. PACHECO, A. PACHECO-VEGA, T. RODIC AND R. E. PECK, *Numerical simulations of heat transfer and fluid flow problems using an immersed-boundary finite-volume method on nonstaggered grids*, Numer. Heat Trans. Part B, 48 (2005), pp. 1–24.
[6] H. F. OZTOP AND E. A. NADA, *Numerical study of natural convection in partially heated rectangular enclosured filled with nanofluids*, Int. J. Heat Fluid Flow, 29 (2008), pp. 1326–1336.
[7] C. SHU, Y. PENG AND Y. T. CHEW, *Simulation of natural convection in a square cavity by taylor series expansion and least squares-based lattice Boltzmann method*, Int. J. Modern Phys. C, 13(10) (2002), pp. 1399–1414.
[8] H. N. DIXIT AND V. BABU, *Simulation of high Rayleigh number natural convection in square cavity using the lattice Boltzmann method*, Int. J. Heat Mass Trans., 49 (2006), pp. 727–739.
[9] Y. PENG, C. SHU AND Y. T. CHEW, *Simplified thermal lattice Boltzmann model for incompressible thermal flow*, Phys. Rev. E, 68 (2003), 026701.
[10] Y. PENG, C. SHU AND Y. T. CHEW, *A 3D incompressible thermal lattice Boltzmann model and its application to simulate natural convection in a cubic cavity*, J. Comput. Phys., 193 (2003), pp. 260–274.
[11] C. S. N. ZWADI AND S. SYAHRULLAL, *A three-dimension double-population thermal lattice bgk model for simulation of natural convection heat transfer in a cubic cavity*, Wseas Trans. Math., 8(9) (2009), pp. 561–571.
[12] Y. PENG, C. SHU AND Y. T. CHEW, *Numerical simulation of natural convection in a concentric annulus between a square outer cylinder and a circular inner cylinder using the Taylor-series-expansion and least-squares-based lattice Boltzmann method*, Phys. Rev. E, 67 (2003), 026701.
[13] Y. SHI, T. S. ZHAO AND Z. L. GUO, *Finite difference-based lattice Boltzmann simulation of natural convection heat transfer in a horizontal concentric annulus*, Comput. Fluids, 35 (2006), pp. 1–15.
[14] Z. G. FENG AND E. E. MICHAELIDES, *The immersed boundary-lattice Boltzmann method for solving fluid-particles interaction problems*, J. Comput. Phys., 194 (2004), pp. 602–628.
[15] C. S. PESKIN, *Flow patterns around heart valves: a numerical method*, J. Comput. Phys., 10(2) (1972), pp. 252–271.
[16] Z. G. FENG AND E. E. MICHAELIDES, *Proteus: a direct forcing method in the simulations of particulate flow*, J. Comput. Phys., 202 (2005), pp. 20–51.
[17] X. D. NIU, C. SHU, Y. T. CHEW AND Y. PENG, *A momentum exchange-based immersed boundary-lattice Boltzmann method for simulating incompressible viscous flows*, Phys. Lett. A, 354 (2006), pp. 173–182.
[18] W. W. REN, C. SHU, J. WU AND W. M. YANG, *Boundary condition-enforced immersed boundary method for thermal flow problems with Dirichlet temperature condition and its applications*, Comput. Fluids, 57 (2012), pp. 40–51.
[19] F. MOUKALLED AND S. ACHARYA, *Natural convection in the annulus between concentric horizontal circular and square cylinders*, J. Thermophys. Heat Trans., 10 (1996), pp. 524–531.